PERGAMON

International Journal of Solids and Structures 38 (2001) 5019–5039

INTERNATIONAL JOURNAL OF SOLIDS and STRUCTURES

www.elsevier.com/locate/ijsolstr

On nonisothermal elastoplastic analysis of shell components employing realistic hardening responses

Zdenko Tonković [a], Jurica Sorić [a,*], Wilfried B. Krätzig [b]

[a] *Faculty of Mechanical Engineering and Naval Architecture, University of Zagreb, I. Lučića 5, 10 000 Zagreb, Croatia*
[b] *Institute for Statics and Dynamics, Ruhr University Bochum, Universitätsstraße 150, D-44780 Bochum, Germany*

Received 17 May 2000; in revised form 31 August 2000

Abstract

In the present paper, efficient numerical algorithms for elastoplastic analysis of shell-like structural components will be proposed employing nonisothermal, realistic, highly nonlinear hardening responses. The closest point projection integration algorithm is presented using a Reissner–Mindlin type kinematic shell model, completely formulated in tensor notation. Further, a consistent elastoplastic tangent modulus is derived, which ensures high convergence rates in the global iteration approach. The integration algorithm has been implemented into a layered assumed strain isoparametric finite element, which also enables geometrical nonlinearities including finite rotations. The nonisothermal elastoplastic response of a circular cylindrical shell and a box column under axial compression is analysed. Under the assumption of an adiabatic process, the increase in temperature is computed during elastoplastic deformation. Robustness and numerical stability of the proposed algorithms are demonstrated.

Keywords: Shell structures; Finite element analysis; Elastoplasticity; Nonisothermal hardening responses; Integration algorithm; Tensor formulation

1. Introduction

The use of thin shells as structural elements in many engineering applications is advantageous due to their high strength to weight ratio. Experimental data and approximate theoretical predictions of deformation processes of metal structures under different types of loading conditions have been presented in a large variety of literature in recent past. Therein, the crushing problem of thin-walled structural elements has attracted considerable attention because of their ability to absorb vast amounts of energy during inelastic structural collapse (Reid, 1993; Reddy and Zhang, 1993; Wierzbicki et al., 1994). Also cyclic elastoplastic responses have been investigated occasionally. As presented in the literature, special interest is directed mainly to the determination of the load–deflection characteristics, evaluation of stress profiles

* Corresponding author. Fax: +385-1-61-68-187.
E-mail addresses: ztonkov@fsb.hr (Z. Tonković), jurica.soric@fsb.hr (J. Sorić), wilfried.b.kraetzig@sd.ruhr-uni-bochum.de (W.B. Krätzig).

0020-7683/01/$ - see front matter
PII: S0020-7683(00)00336-X

along cross-sections and amounts of energy absorbed. It has been recognized that especially nonisothermal material descriptions play a significant role during inelastic deformation processes (Lehmann, 1987; Szepan, 1989).

An accurate modelling of elastoplastic material responses together with geometrical nonlinearities represents the key for describing deformation processes in realistic manner. Employing thermomechanical coupling as under consideration can significantly contribute to the accuracy of numerical simulations. The influence of temperature on the material behaviour may be encompassed in the evolution laws describing hardening responses. Such hardening rules formulated by differential equations are usually applied (Lehmann, 1987; Armstrong and Frederick, 1966; Chaboche, 1986; McDowell, 1992), where the temperature effect has been embedded in the corresponding model parameters. In order to integrate the elastoplastic constitutive model and to obtain the actual state of the stress and of the internal plastic variables, many efficient computational strategies have been developed lately (Auricchio and Taylor, 1994; Auricchio and Taylor, 1995; Chaboche and Cailletaud, 1996; Doghri, 1993; Hartmann and Haupt, 1993; Hopperstad and Remseth, 1995; Montag et al., 1999; Sorić et al., 1997a,b; Sorić et al., 1998). Therein, numerical modelling is mainly performed for two dimensional plane stress and plane strain problems (Doghri, 1993; Hartmann and Haupt, 1993; Hopperstad and Remseth, 1995). An algorithm for modelling of nonlinear hardening responses describing cyclic plasticity of shell structures has first been proposed in Sorić et al. (1998).

The present paper is concerned with the numerical modelling of nonisothermal hardening responses in elastoplastic analyses of shell structures employing a Reissner–Mindlin type kinematic model. The material model employs a highly nonlinear hardening response (Lehmann, 1987) with temperature dependent material functions (Szepan, 1989) obtained experimentally for mild steel. Small strains and an associative flow rule are assumed, and an adiabatic process is considered. The integration algorithm, completely formulated in tensor notation, is based on the closest point projection strategy as proposed in Sorić et al. (1997a), in conjunction with a derived consistent tangent operator.

The computational algorithm, based on the simulation strategy presented in Krätzig (1997), has been implemented into a four-noded isoparametric, assumed strain layered finite shell element (Basar et al., 1993). The finite element formulation allows modelling of material nonlinearities combined with geometrically nonlinear responses considering finite rotations. Efficiency of the proposed algorithm is demonstrated by several numerical examples. Thereby, cyclic elastoplastic responses of a circular tube as well as of axial compression of a cylindrical shell and a box column are considered. Assuming an adiabatic deformation process, the increase in temperature is monitored during the elastoplastic collapse simulated. All computations have been performed within the finite element software FEMAS (Beem et al., 1996) developed at the Ruhr-University Bochum.

2. Elastoplastic material model

2.1. Thermal hardening properties

The present material model, described in detail in this section, employs an associative flow rule with evolution laws for hardening variables as proposed by Lehmann (1987) in which the material functions are experimentally determined (Szepan, 1989). The total strain rate $\dot{\gamma}_{ij}$ of this concept is decomposed into the reversible elastic part $\dot{\gamma}^{\mathrm{e}}_{ij}$, the irreversible plastic part $\dot{\gamma}^{\mathrm{p}}_{ij}$ and the thermal part $\dot{\gamma}^{\mathrm{T}}_{ij}$, as follows

$$\dot{\gamma}_{ij} = \dot{\gamma}^{\mathrm{e}}_{ij} + \dot{\gamma}^{\mathrm{p}}_{ij} + \dot{\gamma}^{\mathrm{T}}_{ij}. \tag{1}$$

As customary, the Latin indices herein take the values 1, 2 and 3, in contrast to the Greek indices used in the later considerations, which take the numbers 1 and 2. The rate of stress tensor is defined by the relation

$$\dot{\sigma}^{ij} = C^{ijkl}\dot{\gamma}_{kl}, \tag{2}$$

where C^{ijkl} abbreviates the constitutive tensor describing the material response.

The von Mises-type yield condition may be written in the form

$$F(\sigma^{ij}, \rho^{ij}, a, T) = \left(S^{ij} - \rho'^{ij}\right)\left(S_{ij} - \rho'_{ij}\right) - k^2(a, T) \leqslant 0, \tag{3}$$

where ρ^{ij} denotes the back stress tensor components describing kinematic hardening, and a is the internal isotropic hardening variable. T denotes the process temperature, while S^{ij} and ρ'^{ij} stand for the deviatoric components of the stress and back stress tensors. According to Szepan (1989), the following isotropic hardening model is adopted.

$$k^2(a, T) = b_1 + b_2 a + b_3\left(1 - \mathrm{e}^{b_4 a}\right), \tag{4}$$

where b_1, b_2, b_3 and b_4 are temperature dependent coefficients. The plastic strain rate is expressed in an associative form

$$\dot{\gamma}^{\mathrm{p}}_{ij} = \dot{\lambda}\frac{\partial F(\sigma^{ij}, \rho^{ij}, a, T)}{\partial \sigma^{ij}}, \tag{5}$$

where λ represents the plastic multiplier. The thermal strain components are given as

$$\dot{\gamma}^{\mathrm{T}}_{ij} = \alpha_{\mathrm{T}}\dot{T}\delta_{ij} \tag{6}$$

with α_{T} as thermal expansion coefficient depending on temperature (Szepan, 1989), and with δ_{ij} representing the Kronecker delta. Temperature changes during the elastoplastic deformation process are expressed by the relation

$$\dot{T} = \frac{\xi}{c_p \rho}\left(S^{ij} - \rho'^{ij}\right)\dot{\gamma}^{\mathrm{p}}_{ij}, \tag{7}$$

in which ξ denotes the dissipation function, while c_p and ρ are the specific heat capacity and the mass density, respectively. The values c_p and ρ depend on the actual process temperature, while ξ is assumed to be constant (Szepan, 1989). Temperature changes are obtained from the balance equation for the remaining energy as shown in Lehmann (1987). Herein the terms with the second mixed derivatives of the specific free enthalpy which describe the coupling with the nondissipative external and internal processes are neglected. Also, heat flux is neglected because an adiabatic process is considered. The kinematic hardening component is expressed by the following nonlinear evolutionary equation (Lehmann, 1987)

$$\dot{\rho}'^{ij} = \varsigma\dot{\gamma}^{\mathrm{p}ij} - \chi\rho'^{ij}\sqrt{\dot{\gamma}^{\mathrm{p}k}_{l}\dot{\gamma}^{\mathrm{p}l}_{k}} \tag{8}$$

with ς and χ as material functions. The material function χ is described in dependence on the process temperature by a polynomial expression in Szepan (1989), while values of ς may be obtained from the following nonlinear relation

$$\varsigma = c_1 + c_2\mathrm{e}^{-c_3 A}. \tag{9}$$

Herein c_1, c_2, c_3 are again temperature dependent coefficients, and A denotes the second invariant of the back stress deviator

$$A = \rho'^{ij}\rho'_{ij}. \tag{10}$$

The internal variable in Eq. (3) describing the isotropic hardening phenomenon is assumed in the form

$$\dot{a} = \left(S^{ij} - \rho'^{ij}\right)\dot{\gamma}^{\mathrm{p}}_{ij}. \tag{11}$$

2.2. Further constitutive formulations

Introducing the relative stress deviator

$$\eta'^{ij} = S^{ij} - \rho'^{ij} \tag{12}$$

and its second invariant

$$J_2 = \frac{1}{2}\eta'^{ij}\eta'_{ij}, \tag{13}$$

the yield criterion can be rewritten as

$$F = 2J_2 - k^2(a,T) = 0. \tag{14}$$

The components of the relative stress deviator are expressed in terms of the relative stress components by the relations

$$\eta'^{ij} = \mu^{ij}_{kl}\eta^{kl}, \tag{15}$$

$$\eta'_{ij} = \mu_{ijkl}\eta^{kl}, \tag{16}$$

where μ^{ij}_{kl} and μ_{ijkl} represent the following transformation tensors (Sorić et al., 1997a)

$$\mu^{ij}_{kl} = \delta^i_k\delta^j_l - \tfrac{1}{3}a_{kl}a^{ij}, \tag{17}$$

$$\mu_{ijkl} = a_{ik}a_{jl} - \tfrac{1}{3}a_{ij}a_{kl}, \tag{18}$$

and the relative stress tensor components are defined as

$$\eta^{ij} = \sigma^{ij} - \rho^{ij}. \tag{19}$$

In Eq. (16), a_{kl} and a^{ij} are the covariant and contravariant components of the metric tensor (Basar and Krätzig, 1985). Analogous to Eqs. (15) and (16), the deviatoric components of the stress and the back stress tensors are introduced as

$$S^{ij} = \mu^{ij}_{kl}\sigma^{kl}, \qquad S_{ij} = \mu_{ijkl}\sigma^{kl}, \tag{20}$$

$$\rho'^{ij} = \mu^{ij}_{kl}\rho^{kl}, \qquad \rho'_{ij} = \mu_{ijkl}\rho^{kl}. \tag{21}$$

Connecting Eqs. (13), (15), (16), (20) and (21), the second invariant of the relative stress deviator takes the following form

$$J_2 = \tfrac{1}{2}\mu_{ijkl}\eta^{ij}\eta^{kl}. \tag{22}$$

According to Eq. (5) and after differentiation of the yield function, the plastic strain rate may be then expressed in the form

$$\dot{\gamma}^{\mathrm{p}}_{ij} = 2\dot{\lambda}\mu_{ijkl}\eta^{kl}. \tag{23}$$

By means of Eqs. (11)–(16) and (20)–(23), the rate of the isotropic hardening variable can be broken down in terms of the second invariant of the relative stress deviator, namely

$$\dot{a} = 4\dot{\lambda}J_2 \tag{24}$$

or, according to Eq. (14), in terms of the isotropic hardening function

$$\dot{a} = 2\dot{\lambda}k^2(a,T). \tag{25}$$

The expression for the back stress tensor components can finally be transformed into the following relation

$$\dot{\rho}^{ij} = 2\dot{\lambda}\varsigma\eta^{ij} - \chi\rho^{ij}\sqrt{\dot{\gamma}_l^{\mathrm{p}k}\dot{\gamma}_k^{\mathrm{p}l}}, \tag{26}$$

in which

$$\sqrt{\dot{\gamma}_l^{\mathrm{p}k}\dot{\gamma}_k^{\mathrm{p}l}} = 2\dot{\lambda}k \tag{27}$$

holds with k as the isotropic hardening function $k = k(a, T)$. After comparison of Eq. (7) with Eq. (11) and by means of Eq. (25), the temperature rate may be rewritten in the following form

$$\dot{T} = \frac{2\dot{\lambda}\xi k^2}{c_p\rho}. \tag{28}$$

During the elastoplastic deformation process the following consistency condition must be fulfilled

$$\dot{F} = \frac{\partial F}{\partial\sigma^{ij}}\dot{\sigma}^{ij} + \frac{\partial F}{\partial\rho^{ij}}\dot{\rho}^{ij} + \frac{\partial F}{\partial a}\dot{a} + \frac{\partial F}{\partial T}\dot{T} = 0. \tag{29}$$

Finally, the loading/unloading criterion is expressed by the Kuhn–Tucker condition (Simo and Hughes, 1998) as follows

$$F(\sigma^{ij}, \rho^{ij}, a, T) \leqslant 0, \quad \dot{\lambda} \geqslant 0, \quad \dot{\lambda}F(\sigma^{ij}, \rho^{ij}, a, T) = 0. \tag{30}$$

3. Numerical formulation for Reissner–Mindlin shell kinematics

3.1. Integration algorithm

In this section, a closest point projection scheme will be developed for integration of the nonisothermal elastoplastic constitutive model including the nonlinear hardening functions on material point level, with fastest possible convergence. The updated values of the state variables $({}^{n}\sigma^{ij}, {}^{n}\rho^{ij}, {}^{n}a, {}^{n}T)$ at the end of the time step $({}^{n-1}t, {}^{n}t)$ have to be found for given values of the incremental strain tensor components ${}^{n}\overset{+}{\gamma}_{ij}$ and the state variables $({}^{n-1}\sigma^{ij}, {}^{n-1}\rho^{ij}, {}^{n-1}a, {}^{n-1}T)$ at time ${}^{n-1}t$. In the following numerical formulation, the rates of all measures are replaced by their incremental values noted by $\left(\overset{+}{\ldots}\right)$. For notational simplicity, the sign plus over the plastic multiplier, denoting its increment, is omitted.

The updating algorithm relies on the following relations in which all measures again are expressed by tensor components:

$${}^{n}\gamma_{ij} = {}^{n-1}\gamma_{ij} + {}^{n}\overset{+}{\gamma}_{ij}, \tag{31}$$

$${}^{n}\gamma_{ij}^{\mathrm{p}} = {}^{n-1}\gamma_{ij}^{\mathrm{p}} + 2\,{}^{n}\lambda\mu_{ijkl}\,{}^{n}\eta^{kl}, \tag{32}$$

$${}^{n}T = {}^{n-1}T + \frac{2\,{}^{n}\lambda\xi\,{}^{n}k^2}{{}^{n}\left(c_p\rho\right)}, \tag{33}$$

$${}^{n}\gamma_{ij}^{\mathrm{T}} = {}^{n-1}\gamma_{ij}^{\mathrm{T}} + {}^{n-1}\alpha_{\mathrm{T}}\,{}^{n}\overset{+}{T}\delta_{ij}, \tag{34}$$

$$ {}^{n}\sigma^{ij} = {}^{n-1}C^{ijkl}\left({}^{n}\gamma_{kl} - {}^{n-1}\gamma^{\mathrm{p}}_{kl} - {}^{n-1}\gamma^{\mathrm{T}}_{kl}\right) - {}^{n-1}C^{ijkl}\left({}^{n}\overset{+}{\gamma}{}^{\mathrm{p}}_{kl} + {}^{n}\overset{+}{\gamma}{}^{\mathrm{T}}_{\gamma\delta}\right), \tag{35} $$

$$ {}^{n}a = {}^{n-1}a + 2\,{}^{n}\lambda\,{}^{n}k^{2}, \tag{36} $$

$$ {}^{n}\rho^{ij} = {}^{n-1}\rho^{ij} + 2\,{}^{n}\lambda\,{}^{n-1}\varsigma\,{}^{n}\eta^{ij} - 2\chi\,{}^{n}\lambda\,{}^{n}k\,{}^{n}\rho^{ij}, \tag{37} $$

$$ {}^{n}\eta^{ij} = {}^{n}\sigma^{ij} - {}^{n}\rho^{ij}, \tag{38} $$

$$ {}^{n}k^{2}({}^{n}a, {}^{n}T) = b_1 + b_2\,{}^{n}a + b_3\left(1 - \mathrm{e}^{b_4\,{}^{n}a}\right), \tag{39} $$

$$ {}^{n}F = 2\,{}^{n}J_2 - {}^{n}k^{2}({}^{n}a, {}^{n}T) \leqslant 0, \quad {}^{n}\lambda \geqslant 0, \quad {}^{n}\lambda\,{}^{n}F = 0. \tag{40} $$

To avoid severe computational difficulties, it should be noted that the elastic material constants, the thermal expansion coefficient as well as the kinematic hardening variable ς are strictly computed at the end of the previous time step ${}^{n-1}t$ and are then assumed as constant during the actual time step. If the hardening variable ς is taken at time ${}^{n}t$ the difficulties arise because an explicit expression for the components of the relative stress tensors can not be derived in terms of the trial state which is necessary for derivation of one scalar nonlinear equation in the plastic multiplier ${}^{n}\lambda$. For the Reissner–Mindlin type shell kinematics (Basar et al., 1993), all stress and strain measures are described by eight tensor components, $\sigma \in \mathbb{R}^8$, $\gamma \in \mathbb{R}^8$ and $\rho \in \mathbb{R}^8$. In contrast to the standard matrix notation, all nine deviatoric components of the stress and back stress tensor, $\boldsymbol{S} \in \mathbb{R}^9$ and $\rho' \in \mathbb{R}^9$, which are expressed by relations (20) and (21), are explicitly included in the present formulation.

According to the closest point projection computational strategy and in view of Eq. (35), the predictor phase is approximated by

$$ {}^{n}\sigma^{\alpha\beta}_{\mathrm{trial}} = {}^{n-1}\sigma^{\alpha\beta} + {}^{n-1}C^{\alpha\beta\delta\varepsilon}\,{}^{n}\overset{+}{\gamma}_{\delta\varepsilon}, \tag{41} $$

$$ {}^{n}\sigma^{\delta 3}_{\mathrm{trial}} = {}^{n-1}\sigma^{\delta 3} + 2^{n-1}Ga^{\delta\varepsilon}\,{}^{n}\overset{+}{\gamma}_{\varepsilon 3}. \tag{42} $$

As may be observed, the in-plane components presented by Eq. (41) and the shear components in Eq. (42) are expressed separately in order to achieve high numerical efficiency (Sorić et al., 1997a). After onset of plastification, the stress components at the end of the time step are obtained by the relations

$$ {}^{n}\sigma^{\alpha\beta} = {}^{n}\sigma^{\alpha\beta}_{\mathrm{trial}} - {}^{n-1}C^{\alpha\beta\gamma\delta}\left({}^{n}\overset{+}{\gamma}{}^{\mathrm{p}}_{\gamma\delta} + {}^{n}\overset{+}{\gamma}{}^{\mathrm{T}}_{\gamma\delta}\right), \tag{43} $$

$$ {}^{n}\sigma^{\delta 3} = {}^{n}\sigma^{\delta 3}_{\mathrm{trial}} - 2^{n-1}Ga^{\delta\varepsilon}\,{}^{n}\overset{+}{\gamma}{}^{\mathrm{p}}_{\varepsilon 3}. \tag{44} $$

By use of Eq. (23), the plastic strain increment at time ${}^{n}t$ can be expressed by the following tensor components:

$$ {}^{n}\overset{+}{\gamma}{}^{\mathrm{p}}_{\alpha\beta} = 2\,{}^{n}\lambda\mu_{\alpha\beta\gamma\delta}\,{}^{n}\eta^{\gamma\delta}, \tag{45} $$

$$ {}^{n}\overset{+}{\gamma}{}^{\mathrm{p}}_{\delta 3} = 2\,{}^{n}\lambda a_{\delta\varepsilon}\,{}^{n}\eta^{\varepsilon 3}. \tag{46} $$

The additional transverse normal strain component ${}^{n}\overset{+}{\gamma}{}^{\mathrm{p}}_{33}$ is determined from the incompressibility condition ${}^{n}\gamma^{\mathrm{p}j}_{j} = 0$, as follows

$$ {}^{n}\overset{+}{\gamma}{}^{\mathrm{p}}_{33} = -2\,{}^{n}\lambda\mu_{\alpha\beta\gamma\delta}a^{\alpha\beta}\,{}^{n}\eta^{\gamma\delta}. \tag{47} $$

In view of Eq. (34), an expression for the thermal strain components is obtained as

$$ {}^{n}\overset{+}{\gamma}{}^{\mathrm{T}}_{\alpha\beta} = \frac{2\xi^{n-1}\alpha_{\mathrm{T}}\,{}^{n}\lambda^{n}k^{2}}{{}^{n}\left(c_{p}\rho\right)}\delta_{\alpha\beta}. \tag{48} $$

Inserting Eqs. (45) and (48) into Eq. (43), and Eq. (46) into Eq. (44), yields

$$ {}^{n}\sigma^{\alpha\beta} = {}^{n}\sigma^{\alpha\beta}_{\mathrm{trial}} - 2\,{}^{n}\lambda^{n-1}C^{\alpha\beta\rho\lambda}\left(\mu_{\rho\lambda\gamma\delta}\,{}^{n}\eta^{\gamma\delta} + \frac{\xi^{n-1}\alpha_{\mathrm{T}}\,{}^{n}k^{2}}{{}^{n}\left(c_{p}\rho\right)}\delta^{\mathrm{p}}_{\lambda}\right), \tag{49} $$

$$ {}^{n}\sigma^{\alpha 3} = {}^{n}\sigma^{\alpha 3}_{\mathrm{trial}} - 4\,{}^{n}\lambda^{n-1}G\,{}^{n}\eta^{\alpha 3}. \tag{50} $$

Applying Eq. (37), the back stress tensor components at time ${}^{n}t$ can be broken down as

$$ {}^{n}\rho^{\alpha\beta} = {}^{n}R^{n-1}\rho^{\alpha\beta} + 2\,{}^{n}R\,{}^{n}\lambda^{n-1}\varsigma^{n}\eta^{\alpha\beta}, \tag{51} $$

$$ {}^{n}\rho^{\delta 3} = {}^{n}R^{n-1}\rho^{\delta 3} + 2\,{}^{n}R\,{}^{n}\lambda^{n-1}\varsigma^{n}\eta^{\delta 3} \tag{52} $$

in which ${}^{n}R$ is introduced as auxiliary variable given by

$$ {}^{n}R = \frac{1}{1 + 2\chi\,{}^{n}\lambda^{n}k}. \tag{53} $$

Now, substituting Eqs. (49) and (51) into Eq. (38) we obtain

$$ {}^{n}\eta^{\gamma\delta}\left(\delta^{\alpha}_{\gamma}\delta^{\beta}_{\delta} - {}^{n}K_{1}a^{\alpha\beta}a_{\gamma\delta}\right) = \frac{{}^{n}K_{2}}{2(1 + 2\,{}^{n}K_{2}\,{}^{n}\lambda^{n-1}G)}\left({}^{n}\eta^{\alpha\beta}_{\mathrm{trial}} - \frac{2\xi^{n-1}\alpha_{\mathrm{T}}\,{}^{n}k^{2n}\lambda}{{}^{n}\left(c_{p}\rho\right)}{}^{n-1}C^{\alpha\beta\rho\rho}\right) \tag{54} $$

with the abbreviations

$$ {}^{n}K_{1} = \frac{2\,{}^{n}K_{2}\,{}^{n}\lambda^{n-1}G(1-2\nu)}{3(1 + 2\,{}^{n}K_{2}\lambda^{n-1}G)(1-\nu)}, \tag{55} $$

$$ {}^{n}K_{2} = \frac{2}{1 + 2\,{}^{n}R\,{}^{n}\lambda^{n-1}\zeta}. \tag{56} $$

The trial relative stress tensor components ${}^{n}\eta^{\alpha\beta}_{\mathrm{trial}}$ are defined by

$$ {}^{n}\eta^{\alpha\beta}_{\mathrm{trial}} = {}^{n}\sigma^{\alpha\beta}_{\mathrm{trial}} - {}^{n}R^{n-1}\rho^{\alpha\beta}. \tag{57} $$

In the program coding of the procedure presented above, the following inverse relation obviously will be particularly useful (Sorić et al., 1997b)

$$ \left(\delta^{\alpha}_{\gamma}\delta^{\beta}_{\delta} - {}^{n}K_{1}a^{\alpha\beta}a_{\gamma\delta}\right)^{-1} = \delta^{\varepsilon}_{\alpha}\delta^{\omega}_{\beta} - \frac{{}^{n}K_{1}}{2\,{}^{n}K_{1} - 1}a_{\alpha\beta}a^{\varepsilon\omega}. \tag{58} $$

Using Eq. (58) and by means of Eqs. (38), (50), (52) and (54), the explicit expressions for the components of the relative stress tensors are obtained in terms of the trial state

$$ {}^{n}\eta^{\alpha\beta} = {}^{n}A^{\alpha\beta}_{\gamma\delta}\left({}^{n}\eta^{\gamma\delta}_{\mathrm{trial}} - \frac{2\xi^{n-1}\alpha_{\mathrm{T}}\,{}^{n}\lambda^{n}k^{2}}{{}^{n}\left(c_{p}\rho\right)}{}^{n-1}C^{\gamma\delta\varepsilon\varepsilon}\right), \tag{59} $$

$$ {}^{n}\eta^{\delta 3} = \frac{1}{1 + 2^{n}\lambda({}^{n}R^{n-1}\varsigma + 2^{n-1}G)}\,{}^{n}\eta^{\delta 3}_{\text{trial}}, \tag{60} $$

where the transformation tensor ${}^{n}A^{\alpha\beta}_{\gamma\delta}$ is broken down in the form

$$ {}^{n}A^{\alpha\beta}_{\gamma\delta} = \frac{1}{1 + 2^{n}\lambda({}^{n}R^{n-1}\varsigma + 2^{n-1}G)}\left[\delta^{\alpha}_{\gamma}\delta^{\beta}_{\delta} + \frac{4^{n}\lambda^{n-1}G(1-2v)}{4^{n}\lambda G(1+v) + 3(1-v)(1 + 2^{n}\lambda^{n}R^{n-1}\varsigma)}\,a_{\gamma\delta}a^{\alpha\beta}\right] \tag{61} $$

and ${}^{n}\eta^{\delta 3}_{\text{trial}}$ is defined by

$$ {}^{n}\eta^{\delta 3}_{\text{trial}} = {}^{n}\sigma^{\delta 3}_{\text{trial}} - {}^{n}R^{n-1}\rho^{\delta 3}. \tag{62} $$

After inserting Eqs. (59) and (60) into the yield criterion (14), the following nonlinear scalar equation is obtained

$$ {}^{n}F = 2^{n}J_2\left({}^{n-1}\varsigma, {}^{n}R, {}^{n}\lambda, {}^{n}\eta^{\alpha\beta}_{\text{trial}}, {}^{n}\eta^{\delta 3}_{\text{trial}}\right) - k^2({}^{n}a, {}^{n}T) = 0, \tag{63} $$

which has to be solved for ${}^{n}\lambda$. In our case of initially isotropic material, the proposed method yields only one scalar nonlinear equation (63) following the lines proposed recently by Auricchio and Taylor (1995), Hartmann and Haupt (1993), Chaboche and Cailletaud (1996). Eq. (63) is solved by Newton's iteration method, and thus

$$ \lambda^{(i+1)} = \lambda^{(i)} - \frac{F^{(i)}}{\left(\frac{\mathrm{d}F}{\mathrm{d}\lambda}\right)^{(i)}}, \tag{64} $$

where $(i+1)$ abbreviates the current iteration step, and $(\mathrm{d}F/\mathrm{d}\lambda)^{(i)}$ is calculated by

$$ \left(\frac{\mathrm{d}F}{\mathrm{d}\lambda}\right)^{(i)} = \frac{F^{(i)} - F^{(i-1)}}{\lambda^{(i)} - \lambda^{(i-1)}}. \tag{65} $$

During the iteration process of the closest point projection scheme, the unknown auxiliary variable ${}^{n}R$ must be computed, which is performed also numerically by means of the following nonlinear relation obtained from Eqs. (36), (39) and (40)

$$ {}^{n-1}a - a + 2\lambda\left[b_1 + b_2 a + b_3\left(1 - \mathrm{e}^{b_4 a}\right)\right] = 0. \tag{66} $$

For a given value of λ this equation has to be solved for an isotropic hardening variable a in each iteration step by applying the local iteration scheme. After determining a, the values of the variable ${}^{n}R$ and the temperature ${}^{n}T$ can be computed.

Then, after determination of the plastic multiplier, the updated value of the stress tensor as well as all internal variables can be calculated. To avoid spurious unloadings, all state variables will be updated with respect to the previous equilibrium state. In order to preserve numerical efficiency of the global iteration strategy on structural level, an elastoplastic tangent modulus consistent with the integration algorithm has to be derived and applied thereby.

3.2. Consistent elastoplastic tangent modulus

This elastoplastic tangent modulus is gained by linearization of the updated algorithm presented in the previous section. In the following presentation, the left upper index n referring to all state variables at time ${}^{n}t$ will be omitted due to further notational simplicity. Inserting Eq. (41) into Eq. (49), and after differentiation and replacing the trial stress by the actual stress tensor components, the following formula is obtained

$$\mathrm{d}\sigma^{\alpha\beta} = C^{\alpha\beta\rho\lambda}\,\mathrm{d}\gamma_{\rho\lambda} - 2\left(D^{\alpha\beta}_{\gamma\delta}\eta^{\gamma\delta} + \frac{\xi\alpha_{\mathrm{T}}k^2}{c_p\rho}C^{\alpha\beta\rho\rho}\right)\mathrm{d}\lambda - 2\lambda D^{\alpha\beta}_{\gamma\delta}\,\mathrm{d}\eta^{\gamma\delta} - \frac{2\xi\alpha_{\mathrm{T}}\lambda}{c_p\rho}C^{\alpha\beta\rho\rho}\,\mathrm{d}k^2. \tag{67}$$

Analogously, by differentiation of Eq. (50) and further use of Eq. (42), we obtain

$$\mathrm{d}\sigma^{\alpha 3} = 2Ga^{\alpha\rho}\,\mathrm{d}\gamma_{\rho 3} - 4G\eta^{\alpha 3}\,\mathrm{d}\lambda - 4\lambda G\,\mathrm{d}\eta^{\alpha 3}. \tag{68}$$

Differentiation of Eq. (4) leads to

$$\mathrm{d}k^2(a,T) = \frac{\partial k^2}{\partial a}\mathrm{d}a + \frac{\partial k^2}{\partial T}\mathrm{d}T. \tag{69}$$

After some suitable formulae manipulations and formation of derivatives, the following relations for the differential of the isotropic hardening variable and of the actual process temperature are delivered

$$\mathrm{d}a = 4J_2\,\mathrm{d}\lambda + 4\lambda\,\mathrm{d}J_2, \tag{70}$$

$$\mathrm{d}T = \frac{\xi}{c_p\rho}\mathrm{d}a. \tag{71}$$

Forming the derivative of the yield function and by use of Eqs. (70) and (71), an alternative form of the consistency condition can be obtained, namely

$$\mathrm{d}J_2 = K_3\,\mathrm{d}\lambda, \tag{72}$$

where

$$K_3 = \frac{2J_2\left(\frac{\partial k^2}{\partial a} + \frac{\xi}{c_p\rho}\frac{\partial k^2}{\partial T}\right)}{1 - 2\lambda\left(\frac{\partial k^2}{\partial a} + \frac{\xi}{c_p\rho}\frac{\partial k^2}{\partial T}\right)}. \tag{73}$$

By use of Eqs. (69)–(72), the isotropic hardening function will be expressed as

$$\mathrm{d}k^2(a,T) = 4\left(\frac{\partial k^2}{\partial a} + \frac{\xi}{c_p\rho}\frac{\partial k^2}{\partial T}\right)(J_2 + \lambda K_3)\mathrm{d}\lambda. \tag{74}$$

The differential of the back stress tensor components $\mathrm{d}\rho^{\alpha\beta}$ and $\mathrm{d}\rho^{\alpha 3}$, obtained from Eq. (37) by means of Eqs. (73) and (74), may be expressed by the following relation

$$\mathrm{d}\rho^{ij} = \left(2^{i-1}\zeta\eta^{ij} - K_4\chi\rho^{ij}\right)\frac{K_5}{1 + 2\chi\lambda k}\mathrm{d}\lambda + (1 - K_5)\mathrm{d}\sigma^{ij} \tag{75}$$

with the abbreviations

$$K_4 = 2k\frac{1 - \lambda\left(\frac{\partial k^2}{\partial a} + \frac{\xi}{c_p\rho}\frac{\partial k^2}{\partial T}\right)}{1 - 2\lambda\left(\frac{\partial k^2}{\partial a} + \frac{\xi}{c_p\rho}\frac{\partial k^2}{\partial T}\right)}, \tag{76}$$

$$K_5 = \frac{1 + 2\chi\lambda k}{1 + 2\lambda\left(^{i-1}\zeta + \chi k\right)}. \tag{77}$$

Differentiation of Eq. (38) yields

$$\mathrm{d}\eta^{\alpha\beta} = \mathrm{d}\sigma^{\alpha\beta} - \mathrm{d}\rho^{\alpha\beta}, \tag{78}$$

$$\mathrm{d}\eta^{\alpha 3} = \mathrm{d}\sigma^{\alpha 3} - \mathrm{d}\rho^{\alpha 3}. \tag{79}$$

Furthermore, inserting Eqs. (74), (78), (79) and (75) into Eqs. (67) and (68) delivers

$$\mathrm{d}\sigma^{\alpha\beta} = B^{\alpha\beta}_{\gamma\delta}\left(C^{\gamma\delta\varepsilon\zeta}\,\mathrm{d}\gamma_{\varepsilon\zeta} - D^{\gamma\delta}\,\mathrm{d}\lambda\right), \tag{80}$$

$$\mathrm{d}\sigma^{\alpha 3} = K_6\left(a^{\alpha\beta}\,\mathrm{d}\gamma_{\beta 3} - L^{\alpha 3}\,\mathrm{d}\lambda\right), \tag{81}$$

where the following abbreviations are introduced

$$B^{\alpha\beta}_{\gamma\delta} = \frac{1}{1+4GK_5\lambda}\left[\delta^{\alpha}_{\gamma}\delta^{\beta}_{\delta} - \frac{4GK_5\lambda(2\nu-1)}{4GK_5\lambda(\nu+1)-3(\nu-1)}a_{\gamma\delta}a^{\alpha\beta}\right], \tag{82}$$

$$D^{\alpha\beta} = C^{\alpha\beta\gamma\delta}\mu_{\gamma\delta\varepsilon\zeta}L^{\varepsilon\zeta} + \frac{4J_2\xi\alpha_{\mathrm{T}}C^{\alpha\beta\rho\rho}}{c_p\rho\left(1-2\nu\frac{\partial k^2}{\partial a}\right)-2\nu\xi\frac{\partial k^2}{\partial T}}, \tag{83}$$

$$L^{ij} = 2K_5\left(\eta^{ij} + \frac{K_4\lambda\chi}{1+2\lambda\chi k}\rho^{ij}\right), \tag{84}$$

$$K_6 = \frac{2G(2\chi k\lambda+1)}{2\chi k\lambda+1-4G\lambda\left(2K_5\lambda^{i-1}\zeta-2\chi k\lambda-1\right)}. \tag{85}$$

The differential of the plastic multiplier $\mathrm{d}\lambda$ in Eqs. (80) and (81) must be expressed in terms of the strain tensor components. After formation of the derivative of the yield functions and by use of Eqs. (78)–(81), (75) and (22), an explicit expression for the plastic multiplier is obtained as follows:

$$\mathrm{d}\lambda = \frac{K_5\mu_{\vartheta\kappa\lambda\nu}B^{\vartheta\kappa}_{\xi\pi}C^{\xi\pi\gamma\delta}\eta^{\lambda\nu}}{K_3+H_1+2H_2}\mathrm{d}\gamma_{\gamma\delta} + \frac{2K_5K_6\eta^{\varepsilon 3}}{K_3+H_1+2H_2}\mathrm{d}\gamma_{\varepsilon 3} \tag{86}$$

with

$$H_1 = \mu_{\alpha\beta\gamma\delta}\left(K_5B^{\alpha\beta}_{\varepsilon\zeta}D^{\varepsilon\zeta} + M^{\alpha\beta}\right)\eta^{\gamma\delta}, \tag{87}$$

$$H_2 = a_{\alpha\beta}\left(K_5K_6L^{\alpha 3} + M^{\alpha 3}\right)\eta^{\beta 3}, \tag{88}$$

$$M^{ij} = \frac{K_5}{1+2\lambda\chi k}\left(2^{i-1}\zeta\eta^{ij} - K_4\chi\rho^{ij}\right). \tag{89}$$

Finally, substitution of Eq. (86) into Eqs. (80) and (81) yields the following relationships between the stress and strain differential components

$$\mathrm{d}\sigma^{\alpha\beta} = C^{\alpha\beta\gamma\delta}_{\mathrm{ep}}\,\mathrm{d}\gamma_{\gamma\delta} + 2C^{\alpha\beta\varepsilon 3}_{\mathrm{ep}}\,\mathrm{d}\gamma_{\varepsilon 3}, \tag{90}$$

$$\mathrm{d}\sigma^{\alpha 3} = C^{\alpha 3\gamma\delta}_{\mathrm{ep}}\,\mathrm{d}\gamma_{\gamma\delta} + 2C^{\alpha 3\varepsilon 3}_{\mathrm{ep}}\,\mathrm{d}\gamma_{\varepsilon 3}, \tag{91}$$

which then deliver the tensor components of the consistent elastoplastic tangent modulus

$$C^{\alpha\beta\gamma\delta}_{\mathrm{ep}} = B^{\alpha\beta}_{\varepsilon\zeta}\left(C^{\varepsilon\zeta\gamma\delta} - \frac{K_5\mu_{\vartheta\kappa\lambda\nu}D^{\varepsilon\zeta}B^{\vartheta\kappa}_{\xi\pi}C^{\xi\pi\gamma\delta}\eta^{\lambda\nu}}{K_3+H_1+2H_2}\right), \tag{92}$$

$$C^{\alpha\beta\varepsilon 3}_{\mathrm{ep}} = -\frac{K_5K_6B^{\alpha\beta}_{\gamma\delta}D^{\gamma\delta}\eta^{\varepsilon 3}}{K_3+H_1+2H_2}, \tag{93}$$

$$C_{\mathrm{ep}}^{\alpha 3\gamma\delta} = -K_5 K_6 \frac{\mu_{\vartheta\kappa\lambda\nu} L^{\alpha 3} B_{\xi\pi}^{\vartheta\kappa} C^{\xi\pi\gamma\delta} \eta^{\lambda\nu}}{K_3 + H_1 + 2H_2}, \tag{94}$$

$$C_{\mathrm{ep}}^{\alpha 3\varepsilon 3} = \frac{K_6}{2}\left(a^{\alpha\varepsilon} - \frac{2K_5 K_6 L^{\alpha 3}\eta^{\varepsilon 3}}{K_3 + H_1 + 2H_2}\right). \tag{95}$$

It is straightforward to verify that the tensor components C_{ep}^{ijkl} are unsymmetrical with respect to the couple of indices $(i\ j)$ and $(k\ l)$, which has its origin in the nonlinear kinematic hardening model as shown in Auricchio and Taylor (1995), Chaboche and Cailletaud (1996), Hartmann and Haupt (1993), Hopperstad and Remseth (1995). For the evaluation of the stiffness matrix, the unsymmetrical tangent operator will be symmetrized according to the following relation (Sorić et al., 1998)

$$\mathrm{sym}\, C_{\mathrm{ep}}^{ijkl} = \tfrac{1}{2}\left(C_{\mathrm{ep}}^{ijkl} + C_{\mathrm{ep}}^{klij}\right) \tag{96}$$

without losses of physical properties but with some disadvantages in speed of convergence.

4. Numerical examples

The integration algorithm in conjunction with the consistent tangent modulus presented in the previous sections has been implemented into an assumed-strain layered finite element (Basar et al., 1993) within the finite element software FEMAS (Beem et al., 1996). By using this highly modular software code, numerical simulations demonstrating excellent performances of the proposed algorithm have been executed. To implement the material model into the finite element formulation used in this paper, we evaluate the material tensor by numerical integration over the shell thickness h

$$E^{n^{ijkl}} = \int_{-h/2}^{h/2} \left(\xi^3\right)^n C_L^{ijkl}\, \mathrm{d}\xi^3, \quad n = 0, 1, 2, 3, \ldots, \tag{97}$$

where C_L^{ijkl} represents the consistently linearized constitutive tensor of layer L, and ξ^3 is the thickness coordinate. The layers are defined by the integration points. In this computation 10 integration points are used in thickness direction. The deformed shell continuum is described by five independent variables, three displacement components and two rotations, which are approximated by standard bilinear interpolation functions (Basar et al., 1993). Material nonlinearity was combined with the modelling of geometrically nonlinear responses assuming finite rotations. For tracing load–displacement curves, Newton–Raphson and Riks–Wempner–Wessels iteration schemes, both enhanced by line search procedures (Montag et al., 1999), were applied. For the constitutive model presented, the material parameters, obtained experimentally for German mild steel St37.12, are taken from Szepan (1989). The Young's modulus of elasticity E and the Poisson's ratio v at the initial temperature of 25°C (298.15 K) have the values of $E = 212$ GPa and $v = 0.285$. The initial yield stress is $\sigma_{\mathrm{Y}} = 240$ MPa. All material parameters depend on the temperature and they are changed during the deformation process. Computations are carried out at different initial temperatures, whereby the temperature changes are considered assuming adiabatic deformation processes.

4.1. Circular tube under torsion

A clamped circular tube subjected to torsion is analysed as first example. The whole cylinder is discretized into 20×20 elements, as shown in Fig. 1 presenting the geometry, loading and finite element mesh. The applied twisting moment produces a shear strain amplitude of ± 0.03 at the free end of the cylinder. In order to test the accuracy of the numerical algorithm, the stress–strain curve presenting one hysteresis loop,

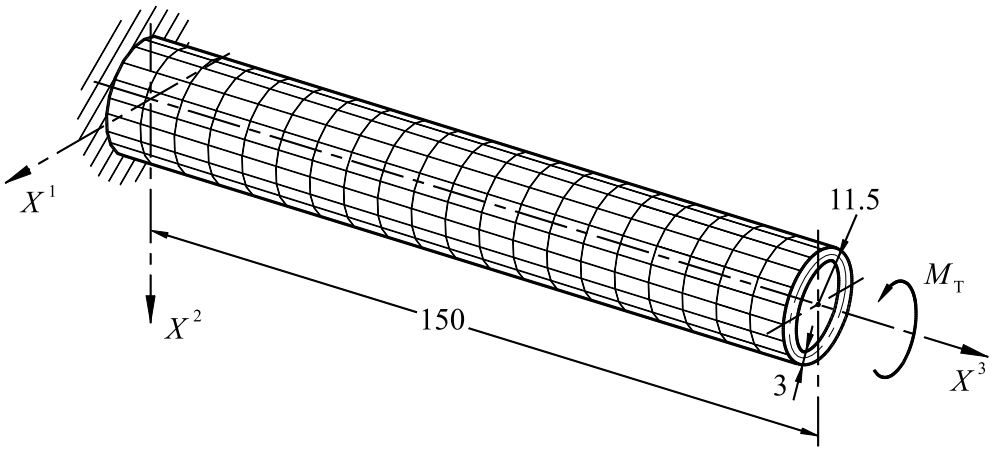

Fig. 1. Geometry and finite element mesh for a circular tube.

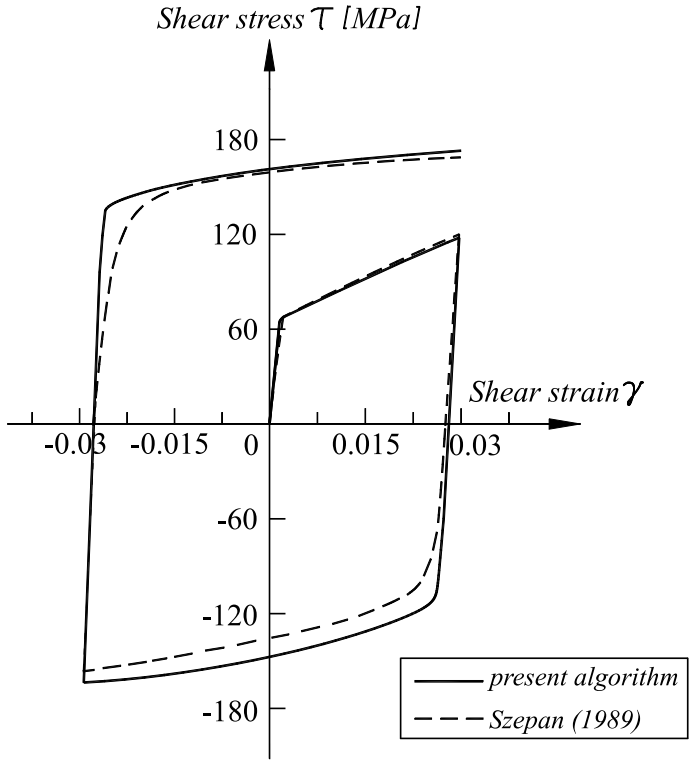

Fig. 2. Shear stress versus shear strain at free end of a circular tube.

computed at the initial temperature of 400°C, is compared with results of experimental investigations obtained in Szepan (1989). As may be observed from Fig. 2, excellent agreement of the two solutions is exhibited. At the end of a full cycle, a temperature increase of 6.2°C has been evaluated.

4.2. Axial compression of a cylindrical shell

As second example, a thin vertical cylinder is considered, clamped along the bottom circle and compressed on the upper free boundary by an increasing line load with the reference value of $q_0 = 1$ N/mm. Employing symmetry, one quarter of the shell is discretized by 20×80 finite elements. The loading, geometry and finite element mesh are shown in Fig. 3. Computer simulations have been performed for four different initial temperatures, of 25°C, 100°C, 200°C and 400°C, wherefrom load–displacement curves have been plotted. The load factor scaling the reference load versus the axial displacement on the upper boundary is presented in Fig. 4 for various initial temperatures. All curves demonstrate the expected buckling problem. The cylinder collapses at a limit point where folding has been initiated, which is followed by unloading and shortening of the shell. The folding progresses to the axisymmetric buckling mode in the region close to the clamped bottom end. The numerical simulation of the deformation process in the post-failure range was limited by the first contact between two consecutive buckles of the cross-section. As evident from Fig. 4, the limit point decreases with the increase of the initial temperature, and in the post-failure range all curves tend to join. The deformed configuration at the response position noted by A in Fig. 4

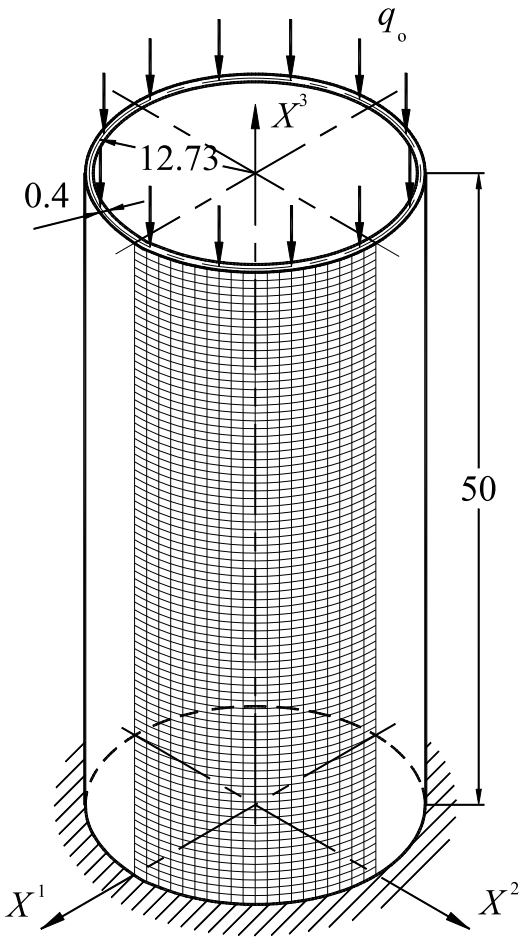

Fig. 3. Geometry and finite element mesh for axially compressed cylindrical shell.

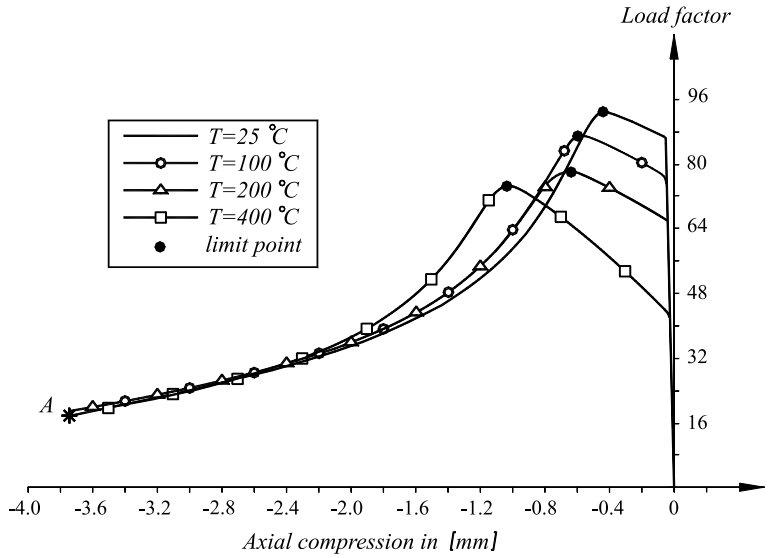

Fig. 4. Load–axial displacement curves for various initial temperatures for the top end of a cylindrical shell.

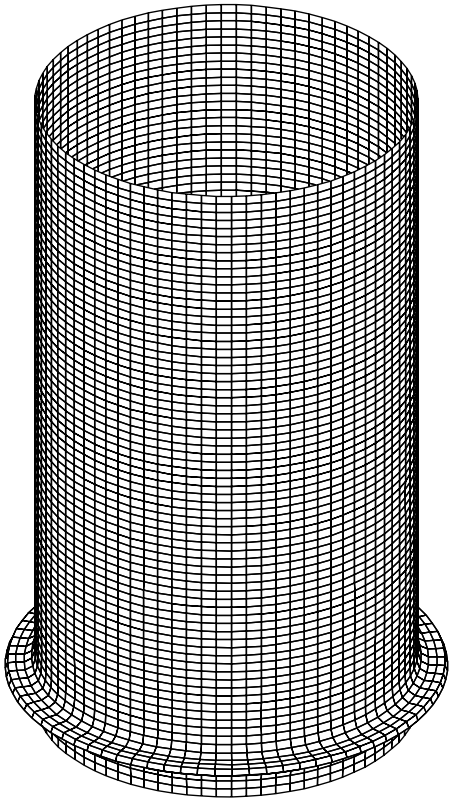

Fig. 5. Deformed configuration for the load level point A.

for an initial temperature of 25°C is depicted in Fig. 5. At the same load level, the plastic zones throughout the deformed shell thickness for four different initial temperatures are shown in Fig. 6, where the layered

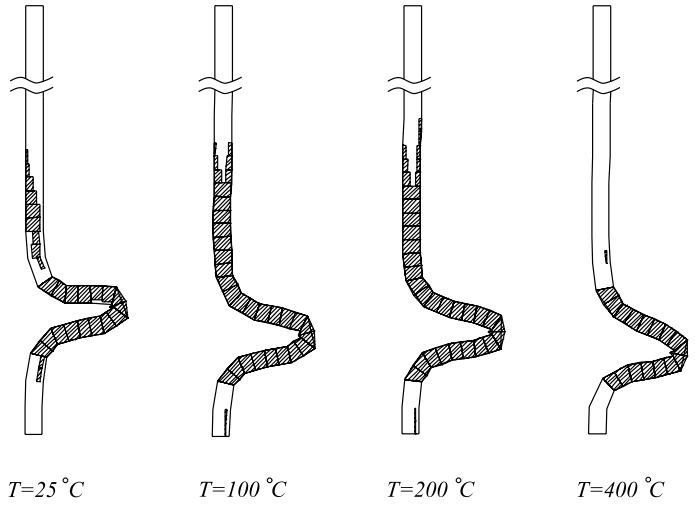

Fig. 6. Spread of plastic zones throughout shell thickness for various initial temperatures for the load level point A.

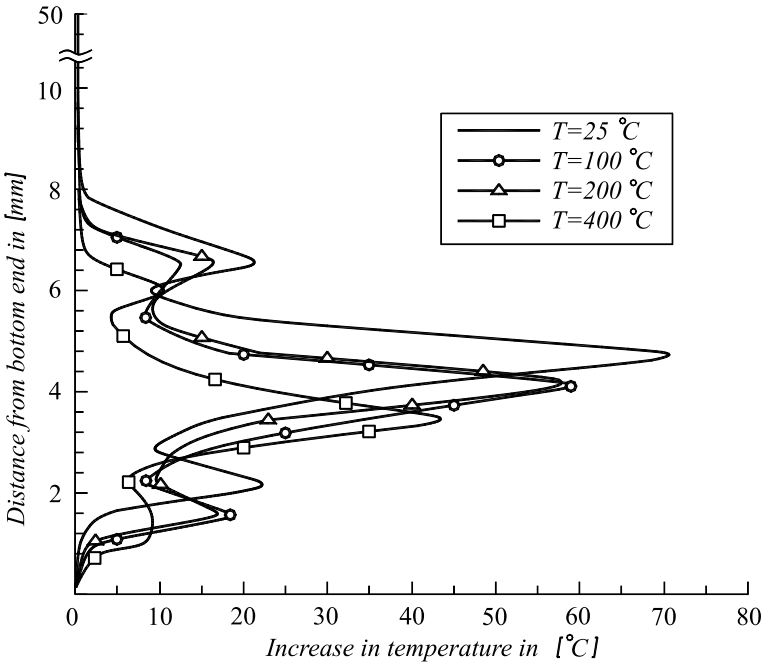

Fig. 7. Temperature increase along the outer shell generatrix for various initial temperatures for the load level point A.

shell sections are plotted only in the regions of plastic actions. It can be easily seen that the minimum plastic region is associated with the largest initial temperature.

As well known, temperatures increase during elastoplastic folding processes. The changes of temperature along the outer shell generatrix for various initial temperatures, for the load level of point A in Fig. 4, are presented in Fig. 7. The temperature distributions are plotted along the outer shell generatrix of the undeformed shell configuration. The largest increase in temperature is associated with the lowest initial temperature, and thus the least temperature increase is exhibited at the largest initial temperature. As expected, the largest increase in temperature is produced in the plastic folding regions undergoing large plastic deformations.

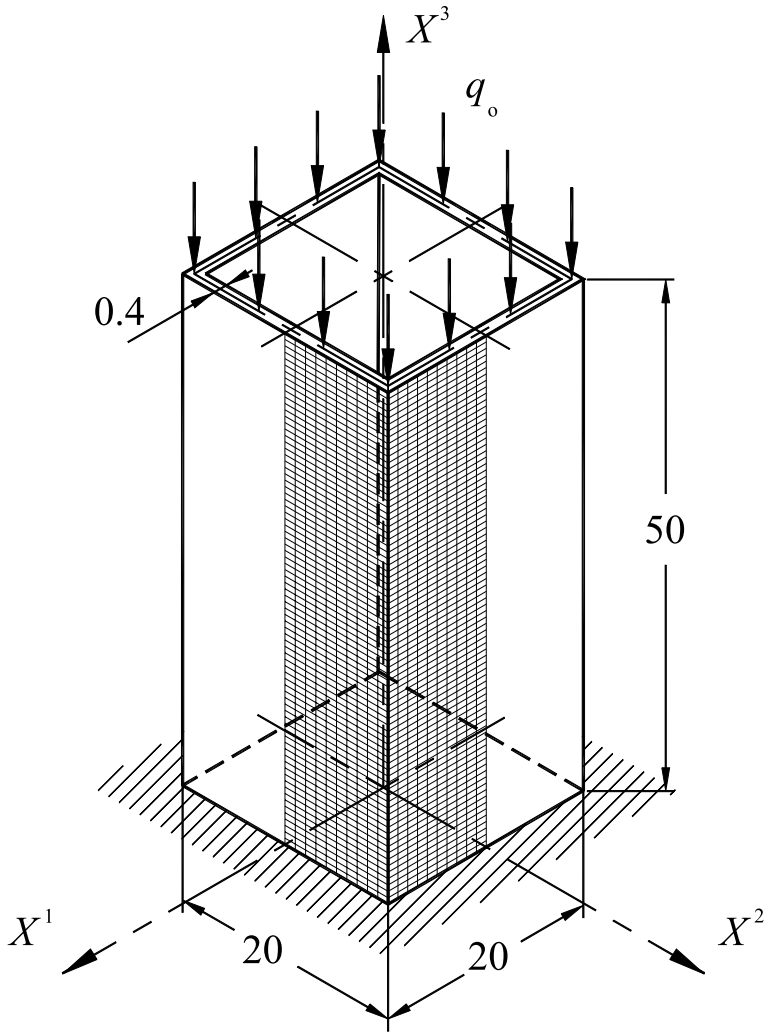

Fig. 8. Geometry, loading and finite element mesh for axially compressed rectangular box column.

4.3. Axial compression of a box column

As last example, axial compression of a rectangular box column will be presented. The column is clamped along the lower boundary and subjected again to the reference compressive line load of $q_0 = 1$ N/mm along the upper end, which will be increased during numerical simulation. The cross-section of the box column, identical with the cross-section of the cylinder considered in the previous example, is chosen in order to compare their deformation responses. Thus, the axial stiffnesses of the box and cylindrical columns are the same. The geometry, loading and finite element mesh are shown in Fig. 8. Considering symmetry again, one quadrant is modelled by a finite element mesh of 20×80, and the computation has been performed only for an initial temperature of 25°C.

The deformation path for one of the corner points on the top end is compared with the curve related to the cylindrical shell in Fig. 9. As obvious, the limit point level on the load–displacement curve of the box column is lower than that one of the deformation response of the cylinder. In the post-buckling range, both curves tend to join. The deformed configuration for the load level point A in the diagram of Fig. 9 is presented in Fig. 10. For the same load level, the plastic zones on the outer column surface are plotted in Fig. 11.

The temperature increases compared with those values obtained for the cylindrical column, again for the same deformation position point A and for an initial temperature of 25°C, is presented in Fig. 12. The temperature distribution for the box column is plotted on the undeformed configuration along two lines of the outer surface, one close to the corner, and the other one close to the symmetry plane of the surface which buckles inwards. It shall be emphasized that there is only a slight difference in temperature increase between the surfaces buckling inwards and outwards. For the cylindrical shell, the change of temperature relates to the outer shell generatrix. For the box girder, the largest increase in temperature occurs close to the corner, in regions undergoing gross plastic deformations. The least temperature increase is along the symmetry plane, where the plastic deformations are significantly smaller. The maximum temperature increase for the cylinder is slightly below the maximum temperature computed for the box column.

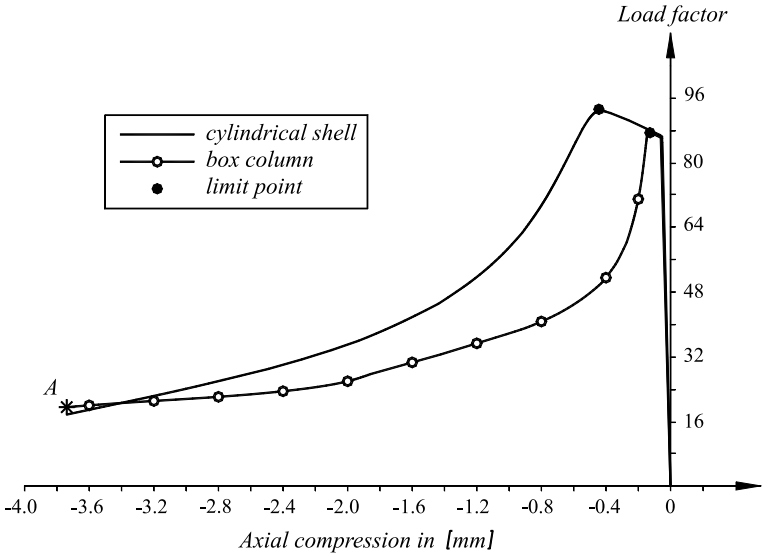

Fig. 9. Load–axial displacement curves for the top end of a box column and a cylindrical shell.

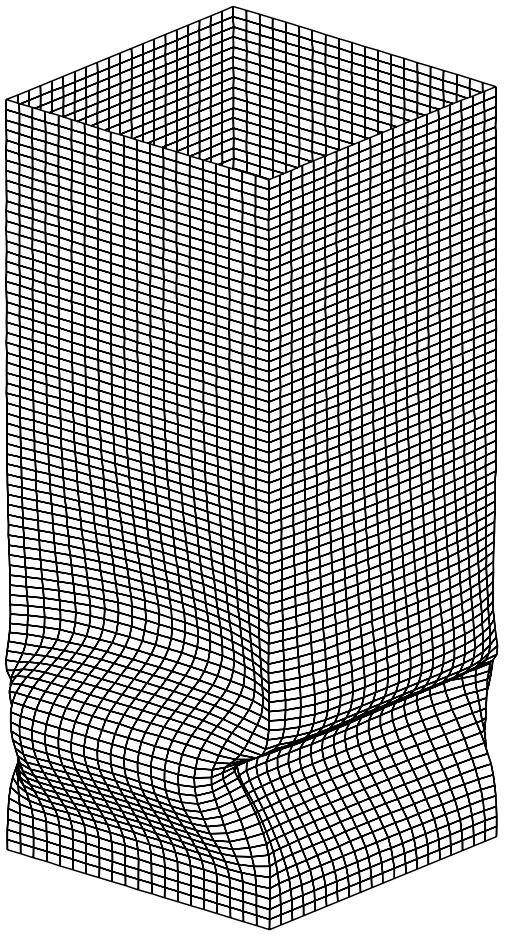

Fig. 10. Deformed configuration of a box column for the load level at point A of the load–displacement curve.

5. Conclusion

An efficient computational strategy for modelling of nonisothermal elastoplastic behaviour of shell and shell-like structures, employing a rather realistic material model with highly nonlinear isotropic and kinematic hardening responses, has been presented. The von Mises-type yield condition expressed in space of stress and temperature, with the assumption of small strain and associativity of the flow rule, has been adopted. A closest point projection algorithm for Reissner–Mindlin type kinematics has been successfully applied. The tensor formulation used allows all nine stress deviator components to be explicitly included in the formulation, which turns out to be an advantage over the classical matrix notation. The derived elastoplastic tangent modulus preserves quadratic convergence rates in the global solution procedures.

Robustness and numerical stability of the proposed algorithms are demonstrated by three numerical examples. The accuracy of the computational procedure has been tested first by comparing the computed stress–strain curve with real experimental data for a circular tube subjected to torsion. Then, influences of initial temperatures on the nonisothermal elastoplastic behaviour of the cylindrical shell under compression

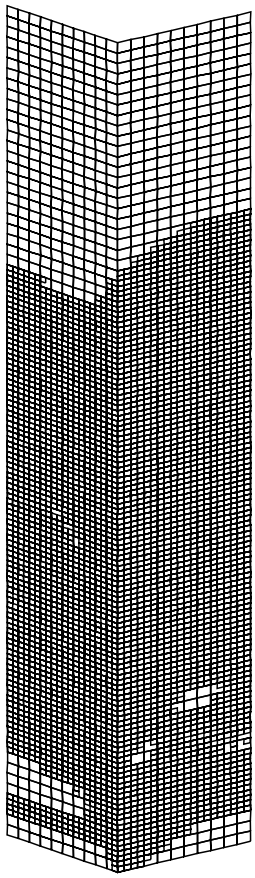

Fig. 11. Plastic zones on the outer column surface for the load level at point A of the load–displacement curve.

are analysed. Assuming adiabatic deformation processes, the increase in the temperature is evaluated and monitored. The increase in temperature slows down with the increase of the initial temperature. The nonisothermal elastoplastic response of the compressed circular shell is finally compared with the deformation process of a box column with same axial stiffness. The maximum temperature increase for the cylinder is slightly below the maximum value associated with the box column. The increase in temperature along the symmetry plane of the box column is significantly smaller than that one computed along the corner.

The numerical analysis of the temperature increase shows clearly that the largest temperature increase occurs in regions undergoing gross plastic deformations, as expected. Clearly, final judgements on the accuracy of the numerical simulation presented may be given only after comparison of the computed results with real experimental data, which do not exist. However, the accurate and efficient modelling of elastoplastic deformation processes of shell-like structural components, employing realistic nonisothermal material hardening responses, can significantly contribute to numerical crash simulations and to the correct prediction of energy absorption devices during collapse processes. In those tasks, in addition to the integration procedure on material point level as described in this paper, the contact problem between consecutive buckles during the elastoplastic folding may require further improvement.

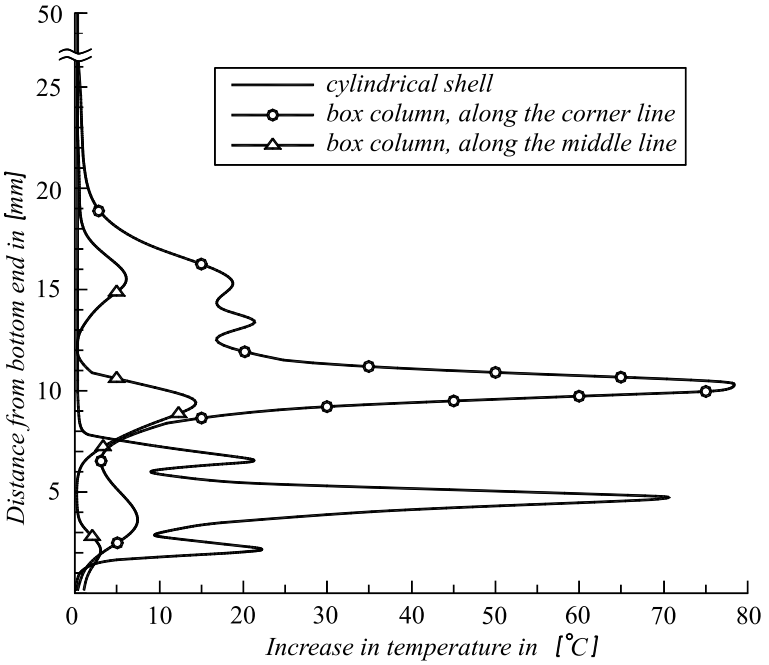

Fig. 12. Comparison of temperature increases of a box column and a cylindrical shell both for point A of the load–displacement curve.

Acknowledgements

The authors express their deep gratitude to the Volkswagen–Stiftung in Hanover, German Science Foundation for their financial support. This work was also supported by the Ministry of Science and Technology of the Republic of Croatia.

References

Armstrong, P.J., Frederick, C.O., 1966. A mathematical representation of the multiaxial Bauschinger effect. GEGB Report No. RD/B/N731, Berceley Nuclear Laboratories.

Auricchio, F., Taylor, R.L., 1994. A generalized elastoplastic plate theory and its algorithm implementation. Int. J. Num. Meth. Engng. 37, 2583–2608.

Auricchio, F., Taylor, R.L., 1995. Two material models for cyclic plasticity: nonlinear kinematic hardening and generalized plasticity. Int. J. Plast. 11, 65–98.

Basar, Y., Krätzig, W.B., 1985. Mechanik der Flächentragwerke. Vieweg, Braunschweig.

Basar, Y., Montag, U., Ding, Y., 1993. On an isoparametric finite element for composite laminates with finite rotations. Comp. Mech. 12, 329–348.

Beem, H., Könke, C., Montag, U., Zahlten W., 1996. FEMAS 2000-finite element modulus for arbitrary structures, Users Manual. Institute for Statics and Dynamics, Ruhr-University Bochum.

Chaboche, J.L., 1986. Time-independent constitutive theories for cyclic plasticity. Int. J. Plast. 2, 149–188.

Chaboche, J.L., Cailletaud, G., 1996. Integration methods for complex plastic constitutive equations. Computat. Meth. Appl. Mech. Engng. 133, 125–155.

Doghri, I., 1993. Fully implicit integration and consistent tangent modulus in elasto-plasticity. Int. J. Num. Meth. Engng. 36, 3915–3932.

Hartmann, S., Haupt, P., 1993. Stress computation and consistent tangent operator using non-linear kinematic hardening models. Int. J. Num. Meth. Engng. 36, 3801–3814.

Hopperstad, O.S., Remseth, S., 1995. A return mapping algorithm for a class of cyclic plasticity models. Int. J. Num. Meth. Engng. 38, 549–564.

Krätzig, W.B., 1997. Multi-level modeling techniques for elasto-plastic structural responses. In: D.R.J. Owen et al. (Eds.), Computational Plasticity, Part 1. CIMNE, Barcelona, pp. 457–468.

Lehmann, Th., 1987. On a generalized constitutive law for finite deformations in thermo-plasticity and thermo-viscoplasticity. In: C.S. Desai, et al. (Eds.), Constitutive Laws for Engineering Materials, Theory and Applications. Elsevier, New York, pp. 173–184.

McDowell, D.L., 1992. A nonlinear kinematic hardening theory for cyclic thermoplasticity and thermoviscoplasticity. Int. J. Plast. 8, 695–728.

Montag, U., Krätzig, W.B., Sorić, J., 1999. Increasing solution stability for finite-element modelling of elasto-plastic shell response, Adv. Engng. Software 30, 607–619.

Reddy, T.Y., Zhang, E., 1993. Effect of strain-hardening on the behaviour of axially crushed cylindrical tubes. In: Lee, W.B. (Ed.), Advances in Engineering Plasticity and its Applications, pp. 755–762.

Reid, S.R., 1993. Plastic deformation mechanisms in axially compressed metal tubes used as impact energy absorbers. Int. J. Mech. Sci. 35, 1035–1052.

Simo, J.C., Hughes, T.J.R., 1998. Computational Inelasticity. Springer, New York.

Sorić, J., Montag, U., Krätzig, W.B., 1997a. An efficient formulation of integration algorithms for elastoplastic shell analyses based on layered finite element approach. Computat. Meth. Appl. Mech. Engng. 148, 315–328.

Sorić, J., Montag, U., Krätzig, W.B., 1997b. On the increase of computational algorithm efficiency for elastoplastic shell analysis. Engng. Computat. 14, 75–97.

Sorić, J., Tonković, Z., Krätzig, W.B., 1998. On numerical simulation of cyclic elastoplastic deformation processes of shell structures. In: Topping, B.H.V. (Ed.), Advances in Finite Element Procedures and Techniques. Civil-Comp Press, Edinburgh, pp. 221–228.

Szepan, F., 1989. Ein elastisch-viskoplastisches Stoffgesetz zur Beschreibung großer Formänderungen unter Berücksichtigung der thermomechanischen Kopplung. Institute for Mechanics, Ruhr-University Bochum.

Wierzbicki, T., Recke, L., Abramowicz, W., Gholami, T., 1994. Stress profiles in thin-walled prismatic columns subjected to crush loading-I. Compression. Comput. Struct. 51, 611–623.